Frequency and angular variations of land surface microwave emissivities: Can we estimate SSM/T and AMSU emissivities from SSM/I emissivities?

Catherine Prigent, Jean-Pierre Wigneron, William B. Rossow, Juan R. Pardo-Carrion

C. Prigent and J. R. Pardo are with Columbia University, NASA Goddard Institute for Space Studies, New York, NY 10025, USA. C. Prigent is on leave from Departement de Radioastronomie Millimetrique, CNRS, Observatoire de Paris, France. J.-P. Wigneron is with the Institut National de la Recherche Agronomique, Station de Bioclimatologie, Agroparc, 84914 Avignon, France. W. B. Rossow is with NASA Goddard Institute for Space Studies, New York, NY 10025, USA

Abstract

To retrieve temperature and humidity profiles from SSM/T and AMSU, it is important to quantify the contribution of the Earth surface emission. So far, no global estimates of the land surface emissivities are available at SSM/T and AMSU frequencies and scanning conditions. The land surface emissivities have been previously calculated for the globe from the SSM/I conical scanner between 19 and 85 GHz. To analyze the feasibility of deriving SSM/T and AMSU land surface emissivities from SSM/I emissivities, the spectral and angular variations of the emissivities are studied, with the help of ground-based measurements, models and satellite estimates. Up to 100 GHz, for snow and ice free areas, the SSM/T and AMSU emissivities can be derived with useful accuracy from the SSM/I emissivities. The emissivities can be linearly interpolated in frequency. Based on ground-based emissivity measurements of various surface types, a simple model is proposed to estimate SSM/T and AMSU emissivities for all zenith angles knowing only the emissivities for the vertical and horizontal polarizations at 53° zenith angle. The method is tested on the SSM/T-2 91.655 GHz channels. The mean difference between the SSM/T-2 and SSM/I-derived emissivities is ≤ 0.01 for all zenith angles with an r.m.s. difference of ≈ 0.02. Above 100 GHz, preliminary results are presented at 150 GHz, based on SSM/T-2 observations and are compared with the very few estimations available in the literature.

Keywords

Microwave radiometry, surface emissivity, ATOVS.

I. Introduction

The Special Sensor Microwave/Temperature 1 and 2 (SSM/T-1 and -2) and the Advanced Microwave Sounding Units A and B (AMSU-A and -B) are both cross-track temperature and water vapor profilers with similar frequencies, but AMSU has better spatial resolution. The SSM/T instruments are on board the Defence Meteorological Satellite Program (DMSP) polar orbiting satellites. SSM/T-1 has 7 channels in the O_2 absorption band around 60 GHz for temperature sounding of the atmosphere [1]. The SSM/T-2 is a water vapor profiler with 5 channels, three in the H_2O absorption line at 183.3 GHz and two window channels at 91.655 and 150 GHz [2]. The Advanced Microwave Sounding Unit (AMSU), part of the Advanced TIROS Operational Vertical Sounder (ATOVS), replaces the Microwave Sounding Unit (MSU) on the previous NOAA polar orbiters. AMSU includes a temperature sounder (AMSU-A) with 15 channels, most of them located in the O_2 absorption band around 60 GHz, and a humidity sounder (AMSU-B) with channels

Microwave land surface emissivities over the globe have been estimated from the Special Sensor Microwave/Imager (SSM/I) observations, by removing the contributions of the atmosphere, clouds and rain using ancillary satellite data [16]-[17]. The SSM/I instrument is described in [18]. Cloud-free SSM/I observations are first isolated with the help of collocated visible/infrared satellite observations (International Satellite Cloud Climatology Project (ISCCP) data [19]. Then, the cloud-free atmospheric contribution is calculated from an estimate of the local atmospheric temperature-humidity profile (National Centers for Environmental Prediction (NCEP) analysis [20]. Finally, with a surface skin temperature derived from IR observations (ISCCP estimate), the surface emissivity is calculated for all the SSM/I channels. The emissivities are estimated for a 53° observation angle at 19.35, 22.235, 37.0 and 85.5 GHz for both vertical and horizontal polarizations with the exception of 22 GHz, which has vertical polarization only. The emissivities are available on a 1/4° grid, compatible with the $\sim 30 \times 30$km ISCCP DX grid and with the SSM/I observations which are sampled at 25 km. The standard deviation of the day-to-day variations of the retrieved emissivities within a month is typically about 0.012 for all the SSM/I frequencies, which is an upper limit on uncertainty of these estimates. Biases arising from uncertainties in the IR emissivity are <0.02.

Similar technics could be applied to SSM/T and AMSU observations to derive the land surface emissivities for each frequency and scanning angle, but because the viewing angles of SSM/T and AMSU are not constant, most scenes on the globe are not seen more than once a month under clear sky conditions with the same angle. Thus, to obtain an adequate climatology, a long time series of data (3 years at least) would have to be processed before having reliable estimates of the natural variability of the surface emissivities. AMSU is now operational since January 1999, and as the data become available, calculations of the emissivities will be performed at the Centre de Meteorology Spatial at Lannion (France) with a method similar to the one developed for SSM/I. However, before an adequate time series of the emissivities become available, some practical alternative has to be implemented now in order to efficiently process the satellite data over land.

We examine the feasibility of estimating the SSM/T and AMSU emissivities over the globe from the previously retrieved SSM/I emissivities, taking into account the different

observations. The $p-$polarized soil emissivity ϵ_{Sp} is given by:

$$\epsilon_{Sp} = 1 - [(1 + \epsilon_{Sp}^{spec}(Q_S - 1) - Q_S \epsilon_{Sq}^{spec}] exp(-h_S \cos^{N_S}(\theta)) \quad (1)$$

where p and q stand for the vertical or horizontal polarizations, ϵ_{Sp}^{spec} is the $p-$polarized specular emissivity; h_S and Q_S are respectively the roughness and the polarization mixing parameters; N_S is an exponent fitted to reproduce the angular variations. The soil dielectric permittivity is calculated from the model described in Calvet *et al.* [22]. The values of the average best fit parameters h_S, Q_S and N_S are given in Table 2 for the three plots and the three frequencies.

To account for the effect of the vegetation canopies, the emissivity ϵ_C of a vegetated surface is computed as follows, for the $p-$polarization:

$$\epsilon_{Cp} = \epsilon_{Sp} \times f_{Sp} + (1 - f_{Sp}) \times \epsilon_V \quad (2)$$

where ϵ_{Sp} is the emissivity of the bare soil calculated from the previous equations, ϵ_V is the emissivity of the vegetation cover, and f_{Sp} is the fraction of bare soil.

The modeling is based on several assumptions. First, it is assumed that the vegetation emissivity simply depends on the crop type and frequency and that it does not depend on polarization and incidence angle. Second, since crops are generally arranged in rows, geometrical effects may be significant. To account for this effect a model is developed for polarization p:

$$f_{Sp} = (1 - \alpha_p \times \tan(\theta)) \times f_{S0} \quad (3)$$

where α_p is a best fit coefficient and f_{S0} is the fractional coverage of soil seen at nadir. However, this last equation can be considered as a modeling refinement for crop covers with row structure and is likely to be unnecessary for large scale footprints which include a variety of surface types.

The simple model described here for vegetation and soil provides a good fit to the available observations with an average r.m.s. error of 0.002 between measured and simulated emissivities. This model is used in our study to analyze the frequency and angular dependence of the land surface emissivities up to 100 GHz.

The RADTRAN surface model calculates vertically and horizontally polarized surface emissivities for various surface types for frequencies up to 40 GHz [24]. The modeling approach for vegetation and bare soil is based on radiative transfer theory where the vegetation is treated as layers of continuous random media bounded by an underlying homogeneous soil layer. The RADTRAN model predicts an increase in emissivity with frequency for vegetation and for bare soil. However, the comparison between simulations and SSM/I data provided in [24] shows that the surface emissivity is somewhat overestimated by the model at 37 GHz (case c in Figure 3 in the paper).

B. From satellite-based estimates

The SSM/I frequencies range from 19 to 85 GHz. For most surfaces, the emissivities in this frequency range vary smoothly with frequency for both orthogonal polarizations at 53^o incidence angle [16]. For nine vegetation classes derived from Matthews [25], Figure 2 shows the frequency dependence of the mean surface emissivity at 53^o zenith angle for each surface type, as calculated for the Meteosat area (Africa plus large portions of Europe and Western Asia) for October 1991. Whatever the vegetation type, the emissivities slowly decrease with frequency for both orthogonal polarizations. For the vertical polarization, the emissivity change between 19 and 85 GHz rarely exceeds 0.05 and is smaller over dense vegetation than over bare soil; for the horizontal polarization, the changes are smaller still (always ≤ 0.025). Under snow and ice conditions, the surface emissivity varies more quickly with frequency and these surface types will have to be studied further.

Alternative estimates of microwave surface emissivities from satellite in this frequency range are scarce. However, all the available estimates from SSM/I observations show that, for various surfaces (bare soil, vegetated soil), the surface emissivity decreases with increasing frequency for both vertical and horizontal polarizations at 53^o incidence. Choudhury [26] analyzed rain forest and desert locations for the period January 1988 to December 1989 and found that emissivities at 37 GHz are almost always lower than at 19 GHz for both orthogonal polarizations. For a 70-day period over the central United States, Jones and Vonder Haar [27] also observed a decrease in emissivity with increasing frequencies from SSM/I measurements at both polarizations. The same trend is confirmed by Xiang and Smith [28] with SSM/I observations of the Sahelian region.

IV. The angular dependence of the microwave land surface emissivities

The SSM/T and AMSU instruments are both cross-track scanners. SSM/T has 7 scan positions θ_s from -39° to +39° and SSM/T-2 has 28 positions from -40.5° to +40.5°. These are satellite view angles which translate into local zenith angles θ_z up to 47.4° near the edge of the scan due to the curvature of the Earth. AMSU-A has 30 scan positions at 3.3° intervals from -14.5×3.3° to +14.5×3.3° while AMSU-B has 90 positions at 1.1° intervals from -44.5×1.1° to +44.5×1.1° which translate into local zenith angles θ_z up to 58.5°. The polarization measured by SSM/T and AMSU rotates with scan angle due to the rotating-reflector/fixed-feed type of antenna design. If θ_s is the scan angle and θ_z is the local zenith angle, then the SSM/T or AMSU surface emissivity $\epsilon(\theta_z)$ seen for a local zenith angle θ_z is given by:

$$\epsilon(\theta_z) = \epsilon_p(\theta_z)\cos^2(\theta_s) + \epsilon_q(\theta_z)\sin^2(\theta_s) \tag{4}$$

$\epsilon_p(\theta_z)$ and $\epsilon_q(\theta_z)$ are the two orthogonal polarized surface emissivities at θ_z local zenith angle. Depending on the channels, p will represent the vertical or the horizontal polarization. The polarization p seen when the incidence is close to nadir (i. e. for θ_z=θ_s very close to 0°) is indicated for each channel on Table 1. θ_s=45° corresponds to θ_z = 53° (which is also the SSM/I zenith angle); for this angle, $\epsilon(53°) = (\epsilon_p(53°) + \epsilon_q(53°))/2$.

The polarization state for SSM/T-2 is sometimes given as "unspecified". In some studies ([29] for instance), SSM/T-2 has been assumed to observe vertical polarization at nadir whereas horizontal polarization at nadir has been assumed by Wessel and Boucher [30] in their comparison of the SSM/I and SSM/T-2 window channels near 90 GHz. From comparisons between observations and simulations, Burns *et al.* [31] concluded that the instrument is observing the horizontal polarization at nadir and this has been confirmed to them by information from the Aerojet system engineers for the SSM/T-2 project.

The SSM/I emissivities are only available at one zenith angle (53°) and for two orthogonal polarizations, giving no information on the emissivity angular dependence.

Model results derived from the INRA measurements are analyzed to estimate the angular dependence of the emissivity. The INRA model is used to simulate the surface emissivities at frequencies up to 100 GHz, for angles between 0° and 60° and for two orthogonal polarizations. The results are presented in Figure 3 for different surface types (smooth

to the cross-track scanners, a single set of coefficients a_n is calculated to minimize the r.m.s. errors between the fitted $F(\epsilon_V(53^\circ), \epsilon_H(53^\circ), \theta_z)$ and the simulated emissivities (solid lines in Figure 3) for all the cases presented in Figure 3. The fit at 90 GHz is added in Figure 3 for each surface type, along with the r.m.s. error between the fit and the model. The r.m.s. error is $\leq$0.015, whatever the surface type. The 'x' symbol in Figure 3 indicates the mean of the two orthogonal polarizations at 53°: The r.m.s. error resulting from the use of this mean value regardless of the zenith angle is indicated in brackets. The r.m.s. error given by the angular dependent function is better or comparable to the r.m.s. error obtained with a fixed mean value. The corresponding a_n coefficients are indicated on Table 3 for 23.8, 36.5 and 90 GHz, for the two possible polarization patterns, i. e. with horizontal or vertical polarizations close to nadir. For each a_n coefficient, a linear regression in frequency is applied and the corresponding $a_n(f)$ are also presented in Table 3 as a function of the frequency f. This is equivalent to applying a linear regression to the whole function.

The function in equation 5 is then tested on different surface types using the RADTRAN model and the $a_n(f)$ previously calculated. The results are presented in Figure 4 for two AMSU-A frequencies. For bare soils and for vegetated areas, the function in equation 5 represents well the model angular dependence, with r.m.s. errors lower than 0.015. For open water surfaces, the angular dependence of the surface emissivity is not well reproduced. These surfaces are characterized by low emissivities at 53° for the horizontal polarization ($\leq$0.5 at 19 GHz): They represent less than 1% of the surface emissivities as calculated from SSM/I and are concentrated in lake or coast areas. These pixels can be processed separately.

V. Verification of the method for SSM/T-2 observations at 91.655 GHz and at frequencies above 100 GHz

Using a linear interpolation in frequency and the angle-dependent model described above, SSM/T and AMSU emissivities up to 100 GHz can be estimated from SSM/I emissivities. We first verify this method against SSM/T observations at 91.655 GHz and then we examine a possible extension of the method above 100 GHz.

SSM/T-2 emissivities at 91.655 GHz and the SSM/I derived emissivities are presented on Figure 5 for three zenith angles. The results obtained when using a mean emissivity calculated at 53°, regardless of the zenith angle, are also shown with dashed lines. When using the angle-dependent model, the mean error (<0.01) and the r.m.s (≈0.02) are similar or lower for all scanning angles than when using the mean emissivity. Note that more than half the r.m.s. differences in Figure 5 can be accounted for by the intrinsic variations in the SSM/I emissivity values; this variability appears in a single month and can be expected to appear year-to-year [16].

B. Possible extension of the method to frequencies above 100 GHz?

Figure 6 presents the 150 GHz emissivities for February 1995 for three zenith angles, along with the emissivity difference between 150 and 91.655 GHz. For desert and sparse vegetation, the emissivities at 150 GHz are lower than at 91.655 GHz. This is not always the case for densely vegetated areas. These results are consistent with Felde and Pickle [29], who also found different spectral variations depending on the surface type. However, as previously mentioned, Hewison [15] found higher emissivity at 150 GHz than at 89 GHz at nadir for all the surfaces they observed. Several $5^o \times 5^o$ areas, where the surface types are supposed to be homogeneous, have been selected to illustrate the angular dependence of the surface emissivities at 91.655 and 150 GHz, as estimated from SSM/T-2 measurements (Figure 7). For each zenith angle, the mean value is indicated along with the associated standard deviation. As expected, at 91.655 GHz, the angular dependence for bare soil and sparse vegetation is stronger than for densely vegetated areas. Despite a large scatter in the results, it appears that the angular dependence of the emissivities over tropical forest is stronger at 150 GHz than at 91 GHz. Over deciduous forests, Hewison [15] also measured a larger than expected angular dependence at 150 GHz (larger than the angular dependence they observe at 89 GHz). At 150 GHz, the standard deviations of the results are larger especially in tropical areas for large zenith angles. This is probably related to the larger atmospheric contribution at this frequency, especially in tropical areas.

Figure 8 shows the change in the estimated emissivity for a given change in the atmospheric contribution (increase in the water vapor continuum absorption or increase in the water vapor column abundance) at 91 and 150 GHz for three standard atmospheres. The

the emissivities can be linearly interpolated in frequency. The scanning and polarization patterns of SSM/T and AMSU are such that the angular dependence of the emissivity seen by these instruments is rather small. Based on ground-based emissivity measurements of various surface types, a simple model is proposed to estimate SSM/T and AMSU emissivities for all zenith angles knowing only the emissivities for the vertical and horizontal polarizations at 53° zenith angle. The method is tested on the SSM/T-2 91.655 GHz channel. The spatial variability of the surface emissivities is well captured. The mean difference between the SSM/T-2 emissivities and the SSM/I derived emissivities at 91.655 GHz is lower than 0.01 for all zenith angles with an r.m.s. difference of ~ 0.02. An atlas of the SSM/I land surface emissivities is available with a $1/4^{\circ}$ resolution. The inter- and intra-annual variability of the emissivities is now under study. With the method developed in this paper, emissivity maps at AMSU-A frequencies and scanning conditions are being prepared for the French Meteorological Office in Lannion (Centre de Meteorologie Spatiale). They will be used as emissivity first guesses in the temperature profile retrieval scheme.

Above 100 GHz, preliminary results have been presented at 150 GHz, based on SSM/T-2 observations. These results are compared with the very few estimations available in the literature. It appears that a simple frequency extrapolation from 90 GHz to 150 GHz will not give satisfactory results. Longer time series of satellite data at 150 GHz will have to be processed, and because of the sensitivity of this frequency to water vapor absorption, special attention will have to be paid to both the water vapor profile estimation and the water vapor absorption model.

ACKNOWLEDGEMENT

We are grateful to M. Rothstein for his help in processing the satellite data sets. NCAR/NCEP Reanalysis data have been provided through the NOAA Climate Diagnostics Center (http://www.cdc.noaa.gov).

REFERENCES

[1] Fleming, H. E., N. C. Grody and E. J. Kratz, *The forward problem and corrections for the SSM/T satellite microwave temperature sounder*, IEEE Trans. Geosc. Remote Sensing, 29, pp.571-584, 1991.

[20] Kalnay, E. et al., *The NCEP/NCAR 40-year reanalysis project*, Bulletin of the American Meteorological Society, 77, pp. 437-470, 1996.

[21] Wang, J. R., B. J. Choudhury, *Remote sensing of soil moisture content over bare field at 1.4 GHz frequency*, Journal of Geophysical Research, 86, pp. 5277-5282, 1981.

[22] Calvet, J.-C., J.-P. Wigneron, A. Chanzy, S. Raju and L. Laguerre, *Microwave dielectric properties of a silt-loam at high frequencies*, IEEE Trans. Geosc. Remote Sensing, 33, pp.634-642, 1995.

[23] Matzler, C., *Passive microwave signatures of landscapes in winter*, Meteorology and Atmospheric Physics, 54, pp. 241-260, 1994.

[24] Isaacs, R. G., Y.-Q. Jin, R. D. Worsham, G. Deblonde and V. J. Falcone, *The RADTRAN microwave surface emission models*, IEEE Trans. Geosc. Remote Sensing, 27, 433-440, 1989.

[25] Matthews, E., *Global vegetation and land use: new high-resolution data bases for climate studies*, J. Clim. Appl. Meteorol., 22, pp. 474-486, 1983.

[26] Choudhury, B. J., *Reflectivities of selected land surface types at 19 and 37 GHz from SSM/I observations*, Remote Sens Environ., 46, pp. 1-17, 1993.

[27] Jones, A. S. and T. H. Vonder Haar, *Retrieval of surface emittance over land using coincident microwave and infrared satellite measurements*, Journal of Geophysical Research, 102, pp. 13609-13626, 1997.

[28] Xiang, X. and E. A. Smith, *Feasibility of simultaneous surface temperature-emissivity retrieval using SSM/I measurements from HAPEX-Sahel*, Journal of Hydrology, 188-189, pp. 330-360, 1997.

[29] Felde, G. W. and J. D. Pickle, *Retrieval of 91 and 150 GHz Earth surface emissivities*, Journal of Geophysical Research, 100, pp. 20855-20866, 1995.

[30] Wessel, J. E. and D. Boucher, *Comparison between cross-track and conical scanning microwave window channels near 90 GHz*, IEEE Trans. Geosc. Remote Sensing, 36, pp. 16-24, 1998.

[31] Burns, B., X. Wu and G. R. Diak, *Impact of emissivity model errors on retrieval of water vapor profiles over ocean with SSM/T2*, paper presented at International Geoscience and Remote Sensing Symposium 98, 1998.

[32] Kleespies, T. J., *Some anomalies in the SSM/T-2 antenna temperatures*, 8th Conference on Satellite Meteorology and Oceanography, American Meteorological Society, pp. 134-136, 1996.

[33] Liebe, H. J., *MPM - An atmospheric millimeter-wave propagation model*, Int. J. Infrared and Millimeter Waves, 10, pp. 631-650, 1989.

[34] English, S. J., C. Guillou, C. Prigent and P. J. Jones, *Aircraft measurements of water vapour continuum absorption at millimetre wavelength*, Quarterly Journal of the Royal Meteorological Society, 120, pp. 603-625, 1994.

[35] Rosenkranz, P W., *Water vapor microwave continuum absorption: a comparison of measurements and models*, Radio Sci., 33, 1998.

Table 1. SSM/T and AMSU characteristics

Channel number	Frequency (GHz)	Polarization at nadir	Resolution at nadir (km)	Atmospheric transmission (tropical)	Atmospheric transmission (winter subarctic)
			SSM/T-1		
1	50.500	H	175	.62	.67
2	53.200	H	175	.20	.22
3	54.350	H	175	.02	.02
4	54.900	H	175	.00	.00
5	58.400	V	175	.00	.00
6	58.825	V	175	.00	.00
7	59.400	V	175	.00	.00
			SSM/T-2		
8	91.655	H	88	.60	.91
9	150.000	H	54	.23	.84
10	183.31±7.00	H	48	.00	.40
11	183.31±3.00	H	48	.00	.07
12	183.31±1.00	H	48	.00	.00
			AMSU-A		
1	23.8	V	50	.78	.99
2	31.4	V	50	.89	.96
3	50.3	V	50	.63	.68
4	52.8	V	50	.29	.32
5	53.596±.115	H	50	.11	.13
6	54.40	H	50	.02	.02
7	54.94	V	50	.00	.00
8	55.50	H	50	.00	.00
9	57.290=ν	H	50	.00	.00
10	ν±.217	H	50	.00	.00
11	$\nu \pm .322 \pm .048$	H	50	.00	.00
12	$\nu \pm .322 \pm .022$	H	50	.00	.00
13	$\nu \pm .322 \pm .010$	H	50	.00	.00
14	$\nu \pm .322 \pm .0045$	H	50	.00	.00
15	89.0	V	50	.61	.91
			AMSU-B		
16	89.0±.9	V	15	.61	.91
17	150.0±.9	V	15	.23	.84
18	183.31±1.00	V	15	.00	.00
19	183.31±3.00	V	15	.00	.07
20	183.31±7.00	V	15	.00	.40

Table 2. Soil parameters for the INRA model

Soil type	Frequency (GHz)	h_{SOIL}	Q_{SOIL}	N_{SOIL}
Smooth soil	23.8	0.43	0.23	0.0
	36.5	0.15	0.33	0.0
	90.0	0.41	0.31	0.0
Rough soil	23.8	0.57	0.43	0.5
	36.5	0.62	0.45	0.5
	90.0	0.71	0.40	0.5
Wheat field	23.8	0.40	0.37	0.0
	36.5	1.00	0.37	0.0
	90.0	0.50	0.40	0.0
		ϵ_{VEG}	α_v	α_h
	23.8	.965	0.43	0.23
	36.5	.980	0.08	1.05
	90.0	.980	0.23	0.23

Table 3. The angular model parameters

Frequency (GHz)	a_0	a_1	a_2	a_3
		V nadir		
23.8	0.13	-5.99e-3	5.21e-4	-0.86e-5
36.5	0.24	-7.56e-3	6.33e-4	-1.09e-5
90.0	0.37	-9.46e-3	7.61e-4	-1.35e-5
f	3.27e-3× f	-4.74e-5× f	3.26e-6× f	-0.66e-7× f
	+0.08	-5.29e-3	+4.75e-4	-0.77e-5
		H nadir		
23.8	0.13	-4.67e-3	-0.07e-4	0.09e-5
36.5	0.24	-6.22e-3	1.04e-4	-0.14e-5
90.0	0.37	-7.61e-3	2.18e-4	-0.40e-5
f	3.27e-3× f	-3.90e-5× f	3.602e-6× f	-0.66e-7× f
	+0.08	-4.21e-3	-0.46e-4	+0.18e-5

Figure 1

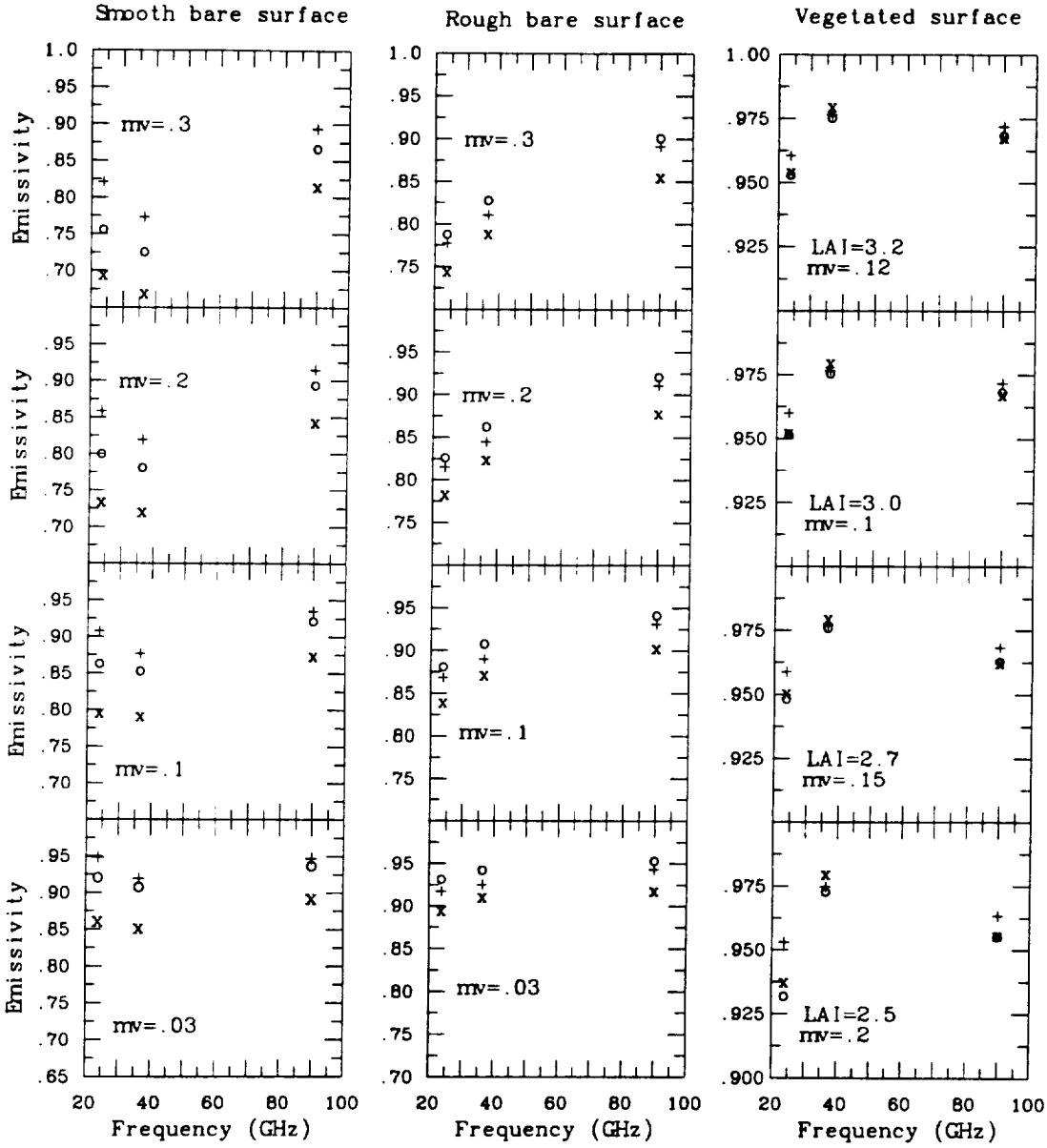
Smooth bare surface
Rough bare surface
Vegetated surface
Emissivity
mv=.3
mv=.2
mv=.1
mv=.03
LAI=3.2
mv=.12
LAI=3.0
mv=.1
LAI=2.7
mv=.15
LAI=2.5
mv=.2
Frequency (GHz)
+ emissivity vertical polarization (53deg)
x emissivity horizontal polarization (53deg)
o emissivity at nadir

Figure 2

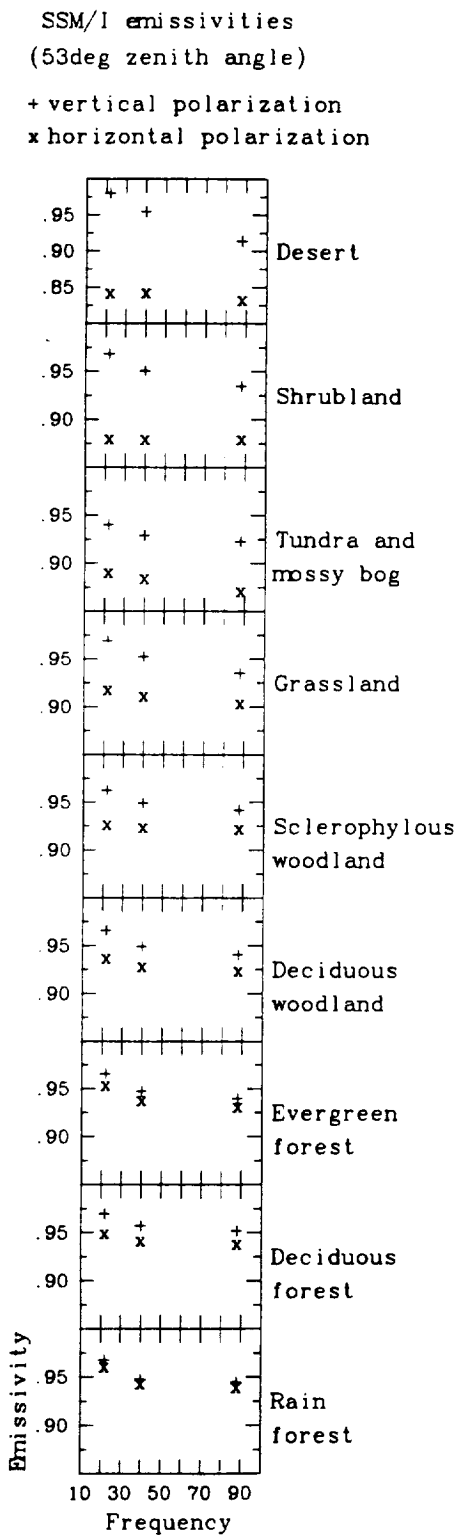
SSM/I emissivities
(53deg zenith angle)
+ vertical polarization
x horizontal polarization
Desert
Shrubland
Tundra and
mossy bog
Grassland
Sclerophylous
woodland
Deciduous
woodland
Evergreen
forest
Deciduous
forest
Rain
forest
Emissivity
.95
.90
.85
10 30 50 70 90
Frequency

Figure 3

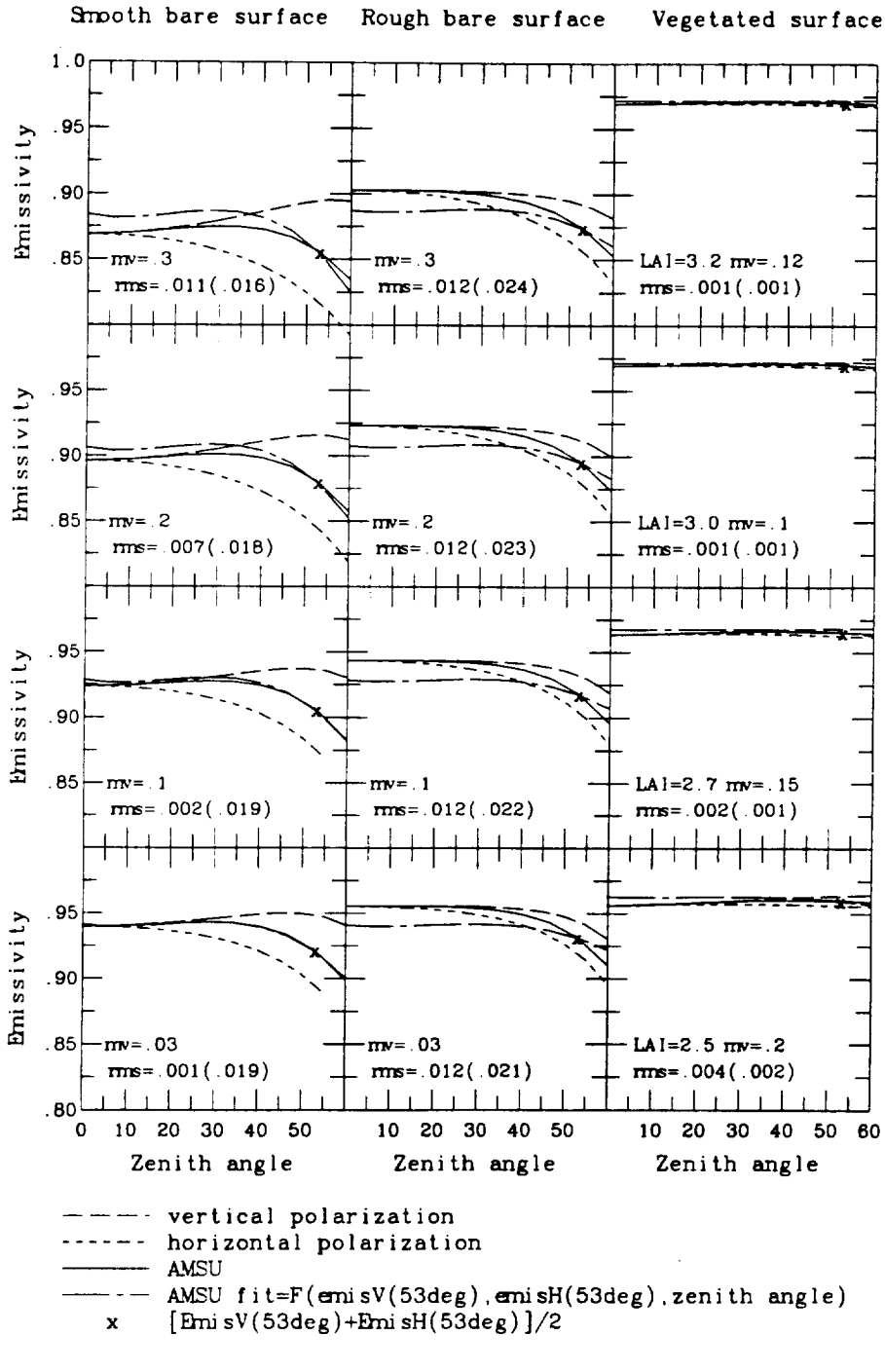
Smooth bare surface
Rough bare surface
Vegetated surface
Emissivity
1.0
.95
.90
.85
.80
mv=.3
rms=.011(.016)
mv=.3
rms=.012(.024)
LAI=3.2 mv=.12
rms=.001(.001)
mv=.2
rms=.007(.018)
mv=.2
rms=.012(.023)
LAI=3.0 mv=.1
rms=.001(.001)
mv=.1
rms=.002(.019)
mv=.1
rms=.012(.022)
LAI=2.7 mv=.15
rms=.002(.001)
mv=.03
rms=.001(.019)
mv=.03
rms=.012(.021)
LAI=2.5 mv=.2
rms=.004(.002)
0 10 20 30 40 50
10 20 30 40 50
10 20 30 40 50 60
Zenith angle
Zenith angle
Zenith angle
vertical polarization
horizontal polarization
AMSU
AMSU fit=F(emisV(53deg),emisH(53deg),zenith angle)
x [EmisV(53deg)+EmisH(53deg)]/2

Figure4

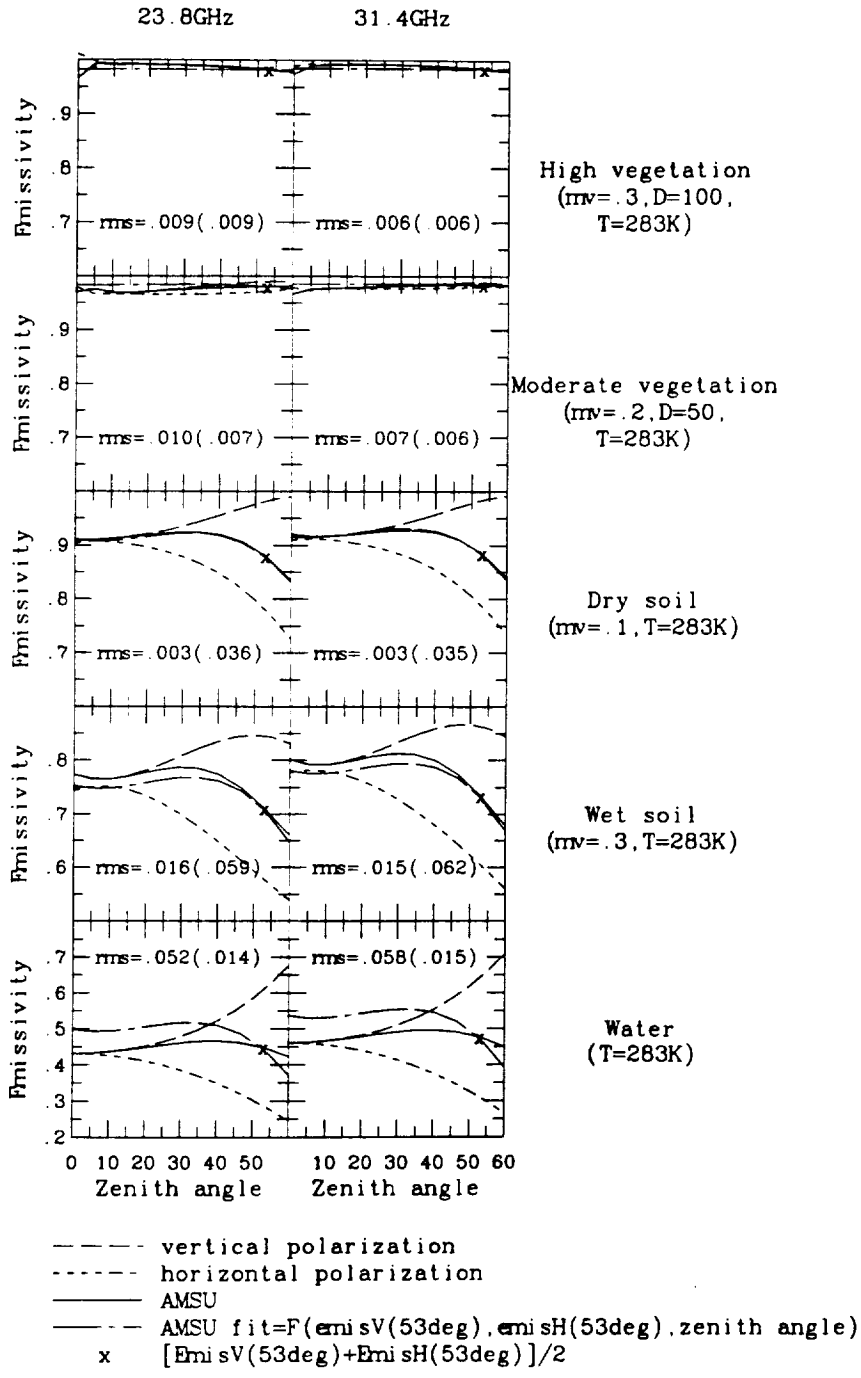
23.8GHz
31.4GHz
Emissivity
rms=.009(.009)
rms=.006(.006)
High vegetation
(mv=.3,D=100,
T=283K)
rms=.010(.007)
rms=.007(.006)
Moderate vegetation
(mv=.2,D=50,
T=283K)
rms=.003(.036)
rms=.003(.035)
Dry soil
(mv=.1,T=283K)
rms=.016(.059)
rms=.015(.062)
Wet soil
(mv=.3,T=283K)
rms=.052(.014)
rms=.058(.015)
Water
(T=283K)
0 10 20 30 40 50
10 20 30 40 50 60
Zenith angle
Zenith angle
vertical polarization
horizontal polarization
AMSU
AMSU fit=F(emisV(53deg),emisH(53deg),zenith angle)
x [EmisV(53deg)+EmisH(53deg)]/2

Fig 5

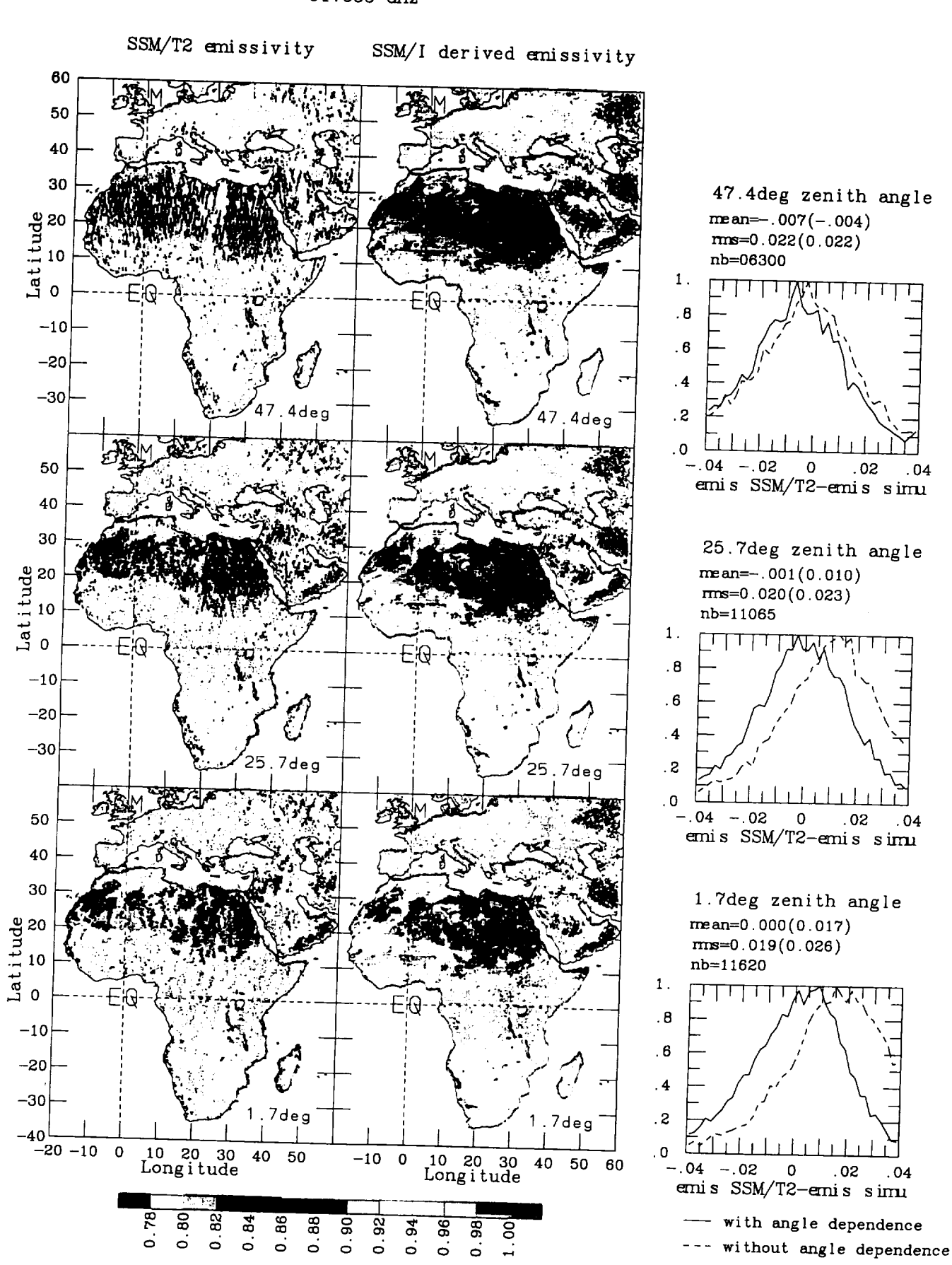
91.655 GHz
SSM/T2 emissivity
SSM/I derived emissivity
Latitude
Longitude
EQ
47.4deg
25.7deg
1.7deg
47.4deg zenith angle
mean=-.007(-.004)
rms=0.022(0.022)
nb=06300
25.7deg zenith angle
mean=-.001(0.010)
rms=0.020(0.023)
nb=11065
1.7deg zenith angle
mean=0.000(0.017)
rms=0.019(0.026)
nb=11620
emis SSM/T2-emis simu
with angle dependence
without angle dependence

Fig 6

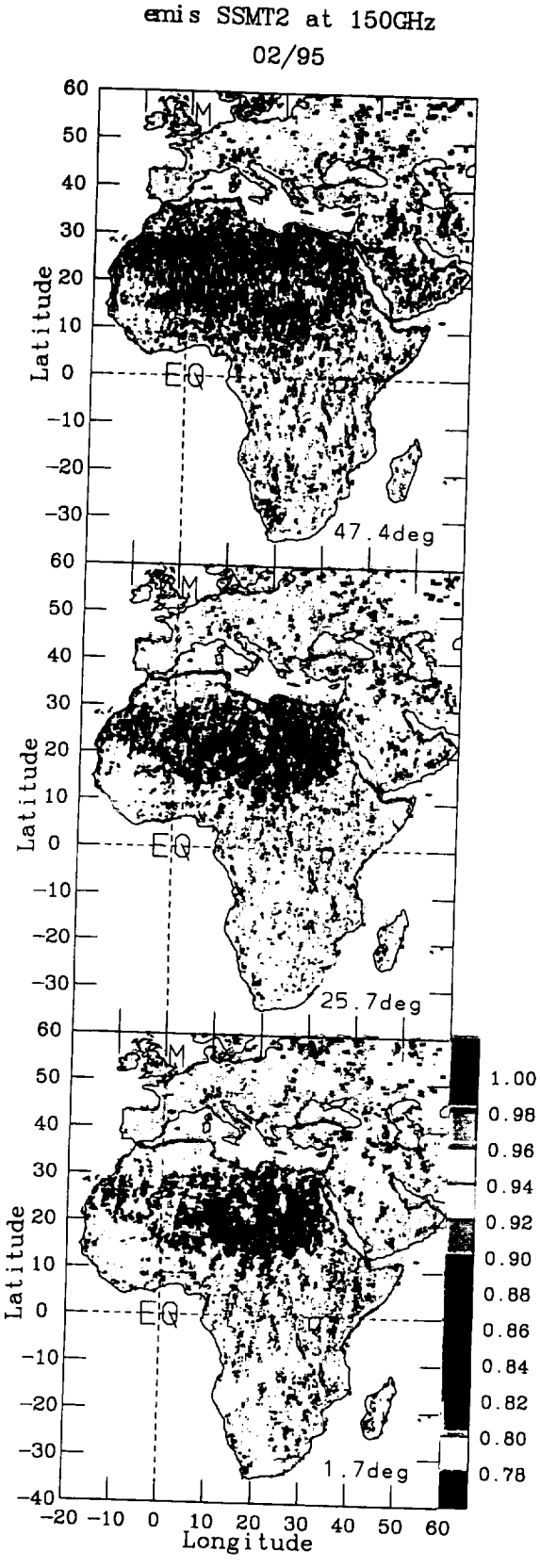
emis SSMT2 at 150GHz
02/95
47.4deg
25.7deg
1.7deg
Latitude
Longitude
1.00
0.98
0.96
0.94
0.92
0.90
0.88
0.86
0.84
0.82
0.80
0.78

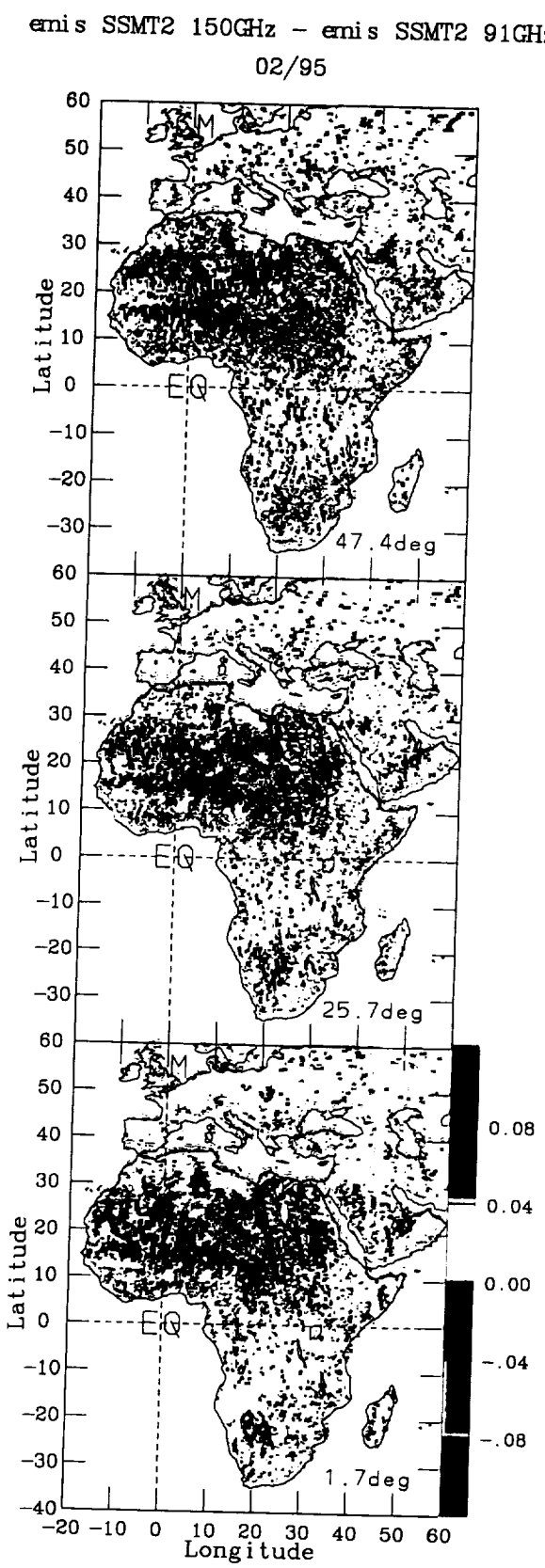
emis SSMT2 150GHz - emis SSMT2 91GHz
02/95
47.4deg
25.7deg
1.7deg
Latitude
Longitude
0.08
0.04
0.00
-.04
-.08

Figure 7

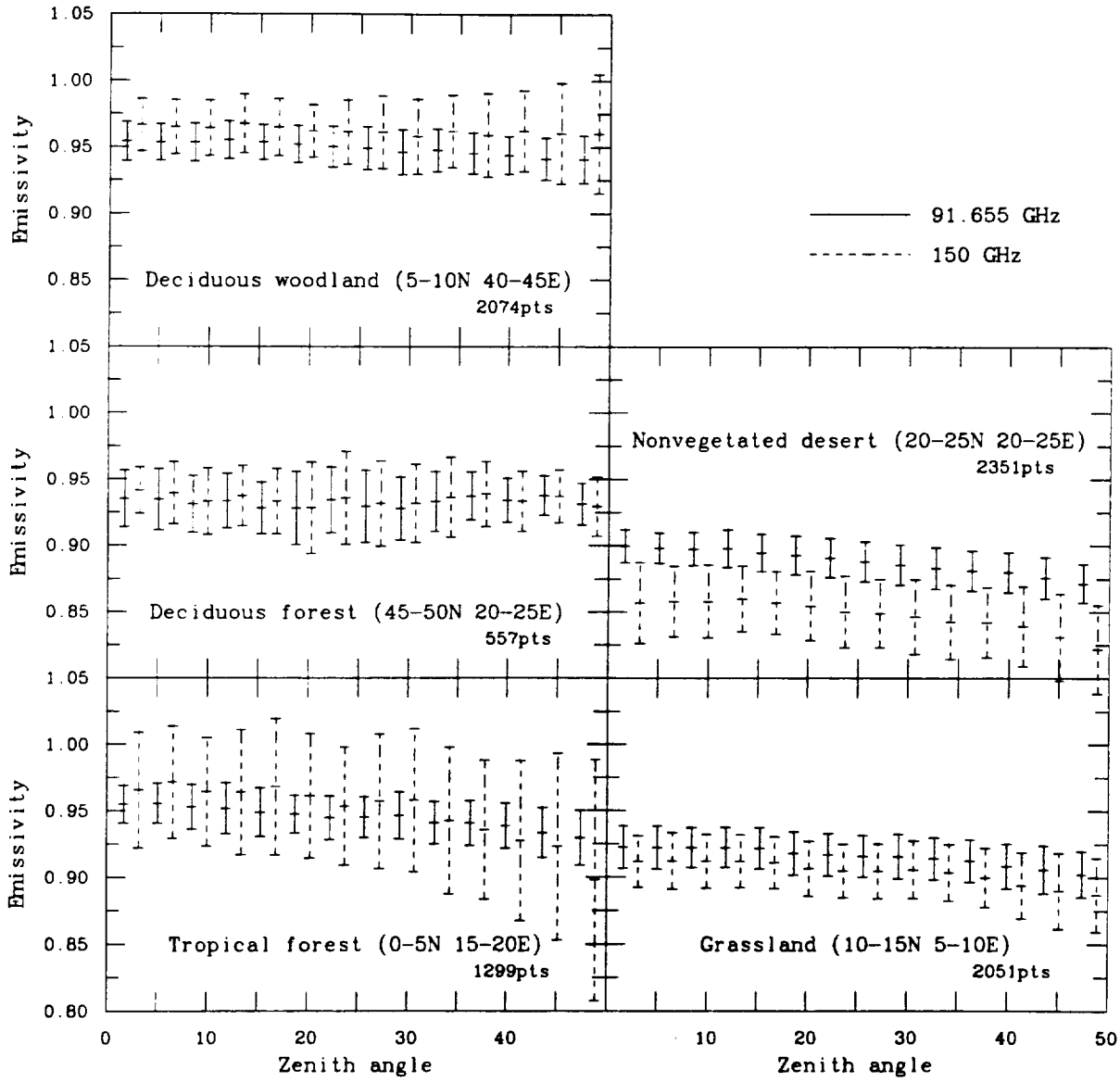
91.655 GHz
150 GHz
Deciduous woodland (5-10N 40-45E)
2074pts
Nonvegetated desert (20-25N 20-25E)
2351pts
Deciduous forest (45-50N 20-25E)
557pts
Tropical forest (0-5N 15-20E)
1299pts
Grassland (10-15N 5-10E)
2051pts
Emissivity
Zenith angle
1.05
1.00
0.95
0.90
0.85
0.80
0
10
20
30
40
50

Figure 8

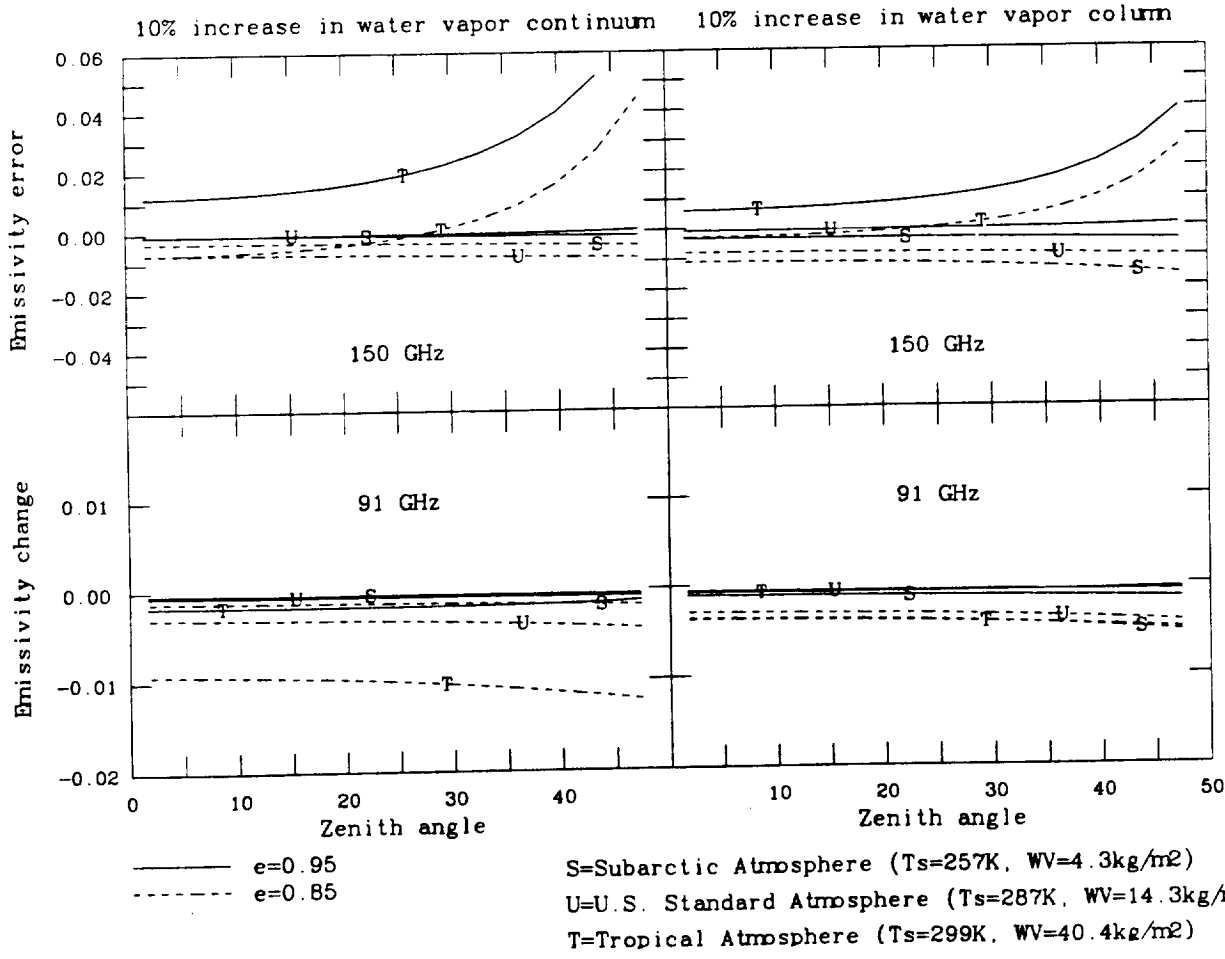
10% increase in water vapor continuum
10% increase in water vapor column
Emissivity error
Emissivity change
150 GHz
91 GHz
Zenith angle
e=0.95
e=0.85
S=Subarctic Atmosphere (Ts=257K, WV=4.3kg/m2)
U=U.S. Standard Atmosphere (Ts=287K, WV=14.3kg/m2)
T=Tropical Atmosphere (Ts=299K, WV=40.4kg/m2)